INTERNATIONAL JOURNAL OF CIRCUITS, SYSTEMS AND SIGNAL PROCESSING
DOI: 10.46300/9106.2022.16.103 Volume 16, 2022

Motion-blurry Image Restoration Method for Detecting Surface Defects of Wood Veneer

Peng Yuan, Liming Lou, Yu Shi, Pengle Cheng*, Lei Yan, Lei Pang
The School of Technology, Beijing Forestry University, Beijing, 100083, China
Corresponding author: Pengle Cheng and Lei Yan

Received: August 28, 2021. Revised: February 13, 2022. Accepted: February 28, 2022. Published: March 11, 2022.

Abstract—The detection of veneer surface defects is of great significance to wood veneer material evaluation, quality control, and product classification in the wood processing. When the high-speed moving veneer image is collected on the conveyor belt, the image appears blurred, making it difficult to accurately identify the defect type and estimate the defect area. To solve this problem, this study compared three image restoration methods including unnatural L0 sparse representation (L0), multi-scale convolutional neural network (MSCNN), and scale-recurrent convolutional neural network (SRCNN). To perform the comparison analysis, a wood veneer image acquisition system was developed and it provided a wood veneer image dataset with 2,080 groups of blur-clear veneer image pairs. Analysis results showed that the SRCNN method performed better than the other two methods. At four different wood moving speeds, the peak signal to noise ratio (PSNR) of the SRCNN was 4.64%, 14.63%, 18.48%, and 25.79%, higher than the other two methods and structural similarity (SSIM) was less than 2%. The average time for this algorithm to restore a blurred wood veneer image was 13.4 s. The findings of this study can lay the foundation for the industrialized detection of wood veneer defects.

Keywords—Wood veneer; Image restoration; Convolutional neural network; Motion blur.

I. Introduction

CHINA is the world's largest producer and exporter of plywood [1]. Defects such as dead knots, joints, holes, and cracks on the surface of the wood veneer directly influence the strength, appearance, and grade of the products, resulting in a price drop in products. Consequently, detecting and removing the surface defects of wood veneers is important for an effective veneer process. The surface defect detection system based on machine vision can potentially detect the type and area of these defects. However, the image blur due to the motion induced during the veneer process significantly lower the detection accuracy of the image analysis methods.

When the single board is moving at high speed, to collect relatively clear images, the camera exposure time needs to be short enough, and at the same time, to ensure the brightness of the image, high-performance camera photosensitive elements are needed. Improving imaging quality will result in excessively higher system costs that cannot meet the production requirements for practical use.

On the other hand, image restoration methods may effectively restore the blurred images that can meet the detection requirements, resulting in improving the accuracy of the real-time detection system for surface defects of the veneer with low costs that is needed for practical applications. Motion blur image is the visible movement of clear image in one direction after a period of time. From the perspective of mathematical models, the convolution of the clear image and the degradation function, and then superimpose the noise function to form a blurred image [2]. The degradation function, also called the point spread function (PSF), is the key to any image restoration.

There are some traditional image restoration methods existing. The restoration method based on multi-frame superposition [3] is effective in removing noise and enhancing the quality of restored images. Later to further improve the quality, a motion blur image restoration algorithm was developed according to unnatural L0 sparse representation (L0) [4]. This algorithm has a good restoration effect on the uniform and non-uniform blur. The motion blur image restoration algorithm can be improved by sparse regularization, which suppresses the ringing effect [5] - [6]. However, traditional image restoration methods are inefficient and require high image quality. In addition, they do not suppress complex noise and introduce noise at strong edges.

With the continuing advances in machine learning, neural network models have been applied to restore images. The neural network models have been used to denoise the original image or the deconvolution processing, which further improves the quality of image restoration [7]. Through combining the image preprocessing with a multilayer perceptron model, the blurred images can be restored with little ringing effect. New image restoration methods based on hybrid neural network were also proposed [8], which had an acceptable restoration efficiency in small-scale blur kernel. A new residual intensive generation of confrontation network image restoration method can effectively extract and restore image edge features and detailed information [9].

[10] compared the single-image deburring with the Neural Networks and evaluated seven NNs for non-blind deblurring (NBD), and seven NNs and four optimization techniques for

blind deblurring (BD). [11] proposed a Deep Pyramid Generative Adversarial Network with Local and Nonlocal Similarity Features for Natural Motion Image Deblurring. The algorithm yielded a superior performance against the current state-of-the-art methods on natural motion image deblurring in terms of visual quality and objective index. It can also be used as a unified network for single and dynamic motion image deblurring.

The challenge for real-time detection system for veneer surface defects is the vagueness of moving veneer images. To meet this challenge, the major objective of this paper is to compare the effectiveness of three different motion-blurred veneer image restoration methods, including the unnatural L0 sparse representation (L0), multi-scale convolutional neural network (MSCNN), and scale-recurrent convolutional neural network (SRCNN), and determine the most practical method for real-time defect detection for veneer surface during the production process. To achieve this goal, experiments were run to collect images of 13 veneer samples at five different operation conditions including a static condition for comparison and four different operation speeds.

II. Experimental

A. Design of Wood Veneer Image Acquisition System

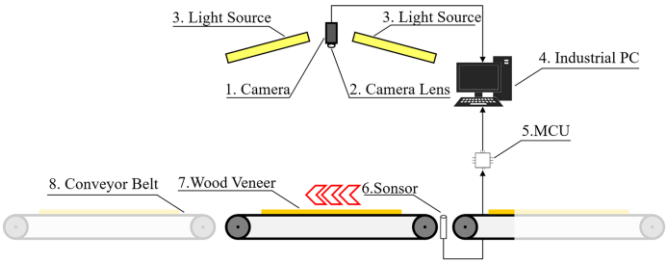

Fig. 1 wood veneer image acquisition system structure diagram.

As shown in Fig. 1, the acquisition system developed in this study to obtain the wood veneer images mainly consist of five components including a camera), a light source, a motion sensor, a micro control unit (MCU), and an industrial computer. The resolution of the used camera is 2456 × 2048, and the pixel size is 3.45 μm2.

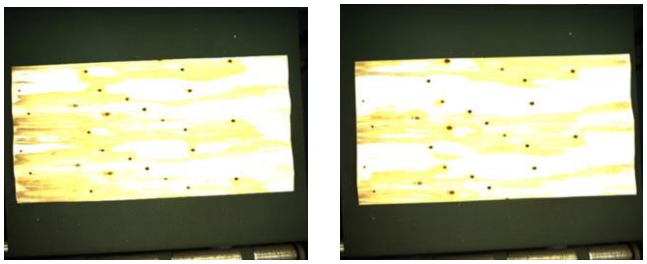

Fig. 2 wood veneer image sample.

The process to acquire the veneer images can be described in two steps as follows: In the first step, the wood veneer cut out from the rotary cutting machine moved forward on the conveyor belt, and when the sensor detected that the wood veneer moved to the specified position, the MCU sent a signal to the industrial computer. Then, the computer would read the wood veneer image collected by the camera. During the experiment, the field of view of the camera should be greater than 1.56 × 1.56 m. Fig. 2 shows two examples of the obtained wood veneer samples from the camera.

B. Establishing the Wood Veneer Image Data Set

Through actual site investigation in some of the wood processing plants, it was learned that most of the current operating speed of the peeling veneer production line in wood production is between 50m/min and 80m/min. In addition, the actual operating speed is adjusted according to production requirements and production environment. Therefore, in this study, four different peeling veneer operation speeds were investigated including 50m/min, 60m/min, 70m/min, and 80m/min and the images acquired for images acquired for all the four different operation speed. The collected images were RGB color images with a resolution of 2456 × 2048 pixels, and the camera exposure time was set to be 5,000 us.

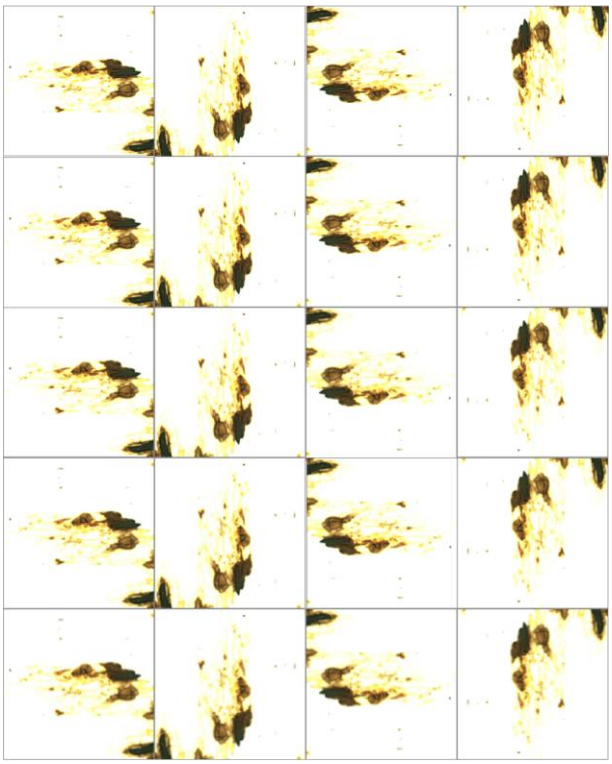

Fig. 3 wood veneer image data set (rows represent five movement status and columns represent four rotation angle): (a) Stationary state, 0°; (b) Stationary state, 90°; (c) Stationary state, 180°; (d) Stationary state, 270°; (e) 50m/min, 0°; (f) 50m/min, 90°; (g) 50m/min, 180°; (h) 50m/min, 270°; (i) 60m/min, 0°; (j) 60m/min, 90°; (k) 60m/min, 180°; (l) 60m/min, 270°; (m) 70m/min, 0°; (n) 70m/min, 90°; (o) 70m/min, 180°; (p) 70m/min, 270°; (q) 80m/min, 0°; (r) 80m/min,;90°; (s) 80m/min, 180°; (t) 80m/min, 270°.

The experiments in this study collected images from 13 wood veneer images in five different states. In addition to the four different operation speeds, images of the wood veneer in the static state were also taken as the clear images as reference groups for comparison. Since the training efficiency of the neural network improves with a smaller image size, in this

paper, the area of each wood veneer was cropped into ten image blocks of 720 × 720 pixels. At the same time, each image block was copied and rotated by 90°, 180°, and 270°. This process would increase the richness of the data set, promote the learning effect of the neural network, and prevent overfitting. As a result, 2,080 groups of clear and fuzzy image pairs were constructed from the experiments. During modeling, the training and testing sets were randomly divided at a ratio of 7:3. Fig. 3 is an example of sample sets in different directions under five states. As the motion speed increased, the image became more blurred.

C. Unnatural L0 Sparse Representation for Image Restoration

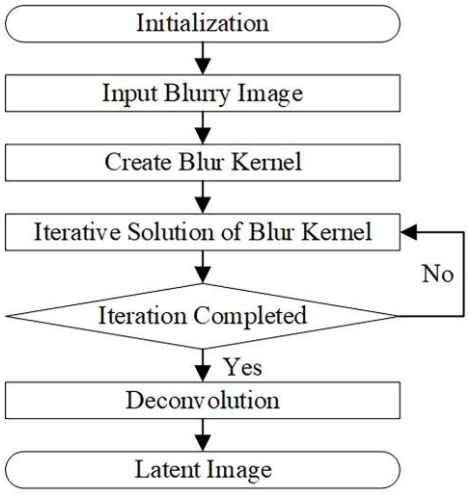

Fig. 4 image restoration method flowchart based on unnatural L0 sparse.

Unnatural L0 sparse (called L0 in this paper) is a method used for image restoration based on the step edge characteristics in unnatural expression [10]. Fig. 4 shows the flow chart of this method. The regularization consists of a series of loss functions that target unnatural L0 sparse, which can keep the energy at a minimum and make the iteration converge quickly.

D. Multi-scale Convolutional Neural Network for Image Restoration

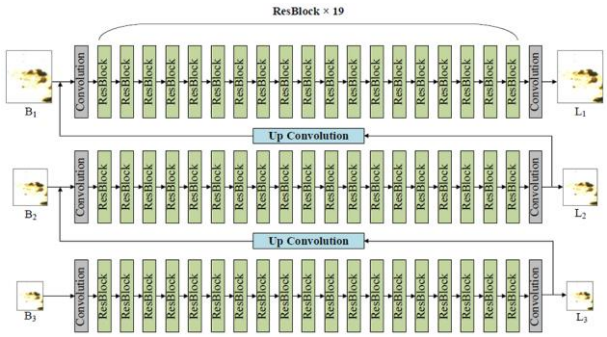

Fig. 5 multi-scale convolutional neural network architecture.

Deep convolutional neural networks can be used for complex non-linear mappings [12] - [15]. Multi-scale convolutional neural network (MSCNN) restores blurry images in an end-to-end manner to solve the estimation problem of blur kernel, and it simulates the multi-scale loss function of the traditional coarse-to-fine method, which improves the convergence speed and is widely used in blurred image restoration [16]. Fig. 5 shows the structure of the MSCNN network. In Fig. 5, Bk and Lk represent the blurred images and potentially clear images, respectively. The subscript k=1,2,3 represents the scale level. Because the four-layer and five-layer Gaussian pyramid networks required longer training time and were difficult to converge [17] - [18], the model adopted a three-layer Gaussian pyramid structure from coarse to fine. B1 was an image block of size 256*256 randomly cropped from the input blurred image. The resolution of the image block decreased successively with the increase of k, and the scale interval ratio was set to 0.5. B1 was down-sampled according to the proportion, so the sizes of B2 and B3 were 128*128 and 64*64, respectively. The network started from the coarse scale and used B3 as input to perform convolution operations (the size of the convolution kernel was 5*5). To keep the input and output sizes consistent during convolution, zero padding was added. The 19 residual blocks were connected after the convolutional layer to remove the linear rectification function after the jump connection in the original residual structure. Then, a convolutional layer was connected to output the restored potentially clear image block, known as L3. The potentially clear image information obtained by the coarse-scale network was transmitted to the clearer-scale network, and the potentially clear image blocks (L3 and L2) was spliced with the blurred image blocks (B2 and B1) to form intermediate scale and clear scale inputs. In contrast to the upsampling method [19] - [21], the MSCNN method made the image blocks output by rough scale, namely L3 and L2, to meet the input requirements of the next scale network through upconvolution. Finally, L1 was the output of the full-size potentially clear image block.

In addition, the Adam optimizer was used in the MSCNN method, and the hyperparameters were set as Beta1=0.9, Beta2=0.999, and $\varepsilon=1\times10^{-9}$. In the network training, a small batch data training method was used with 4 image blocks as input each time. Each round of training contained 364 calculations, for a total of 200 rounds of training. The initial learning rate of the network was set to be 5×10^{-5}, and the rest of the parameters were initialized by the Xavier algorithm [22].

E. Scale-recurrent Convolutional Neural Network for Image Restoration

The scale-recurrent convolutional neural network (SRCNN) optimizes the residual block structure and adds convolutional long short-term memory network (ConvLSTM) to the network. The residual block is added to the coding block and the decoding block, and the coding block and the decoding block based on the residual block are improved. A complete coding block is composed of a convolutional layer, ReLU and three residual blocks. The decoding block is composed of three residual blocks, a deconvolutional layer and ReLU. The decoding block has a symmetrical structure to the encoding block, so adding the same number of encoding and decoding

blocks to the network can make the input data and output data the same size, which makes the encoding and decoding structure widely used in various image processing scenarios. The algorithm expands the receptive field of the network, improves the training efficiency, and increases the utilization of image features [23].

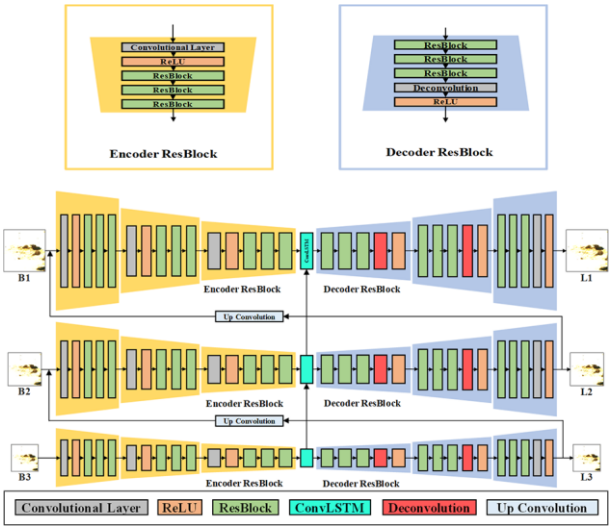

Fig. 6 scale-recurrent convolutional neural network architecture.

Fig. 6 shows a structural diagram of the SRCNN method. First, the blurred image B1 was the input, and the blurred images B2 and B3 were obtained by down-sampling. Then B3 was input from the coarse scale, and the spatial size of the image was minimized through three coding blocks. After the image passed through the ConvLSTM, it retained the hidden layer information to the intermediate scale while continuing to transmit the image data. The spatial size of the image was restored through three decoding blocks, and the deconvolution layer in the last decoding block was replaced with a convolution layer. The potentially clear image L3 that has undergone the up-convolution operation and the intermediate-scale blurred image B2 were jointly used as the intermediate-scale input. When the image data passed through the intermediate-scale ConvLSTM, it continued to transfer the hidden layer information to the clear scale. Meanwhile, it combined the rough-scale hidden layer information to transfer the image data to the decoding block, and then the potentially clear image L2 was obtained from the decoding block.

The size of the convolution kernel in the network was 5 × 5. The step size of the convolution kernel in the last and the first two decoding blocks in each scale was 2, while the step size of the remaining cores was 1. The activation function used in the network was linear rectification function. When the parameters in each scale were different, there was a large number of parameters that need to be trained in the network, which greatly reduced the training efficiency of the network that easily leads to convergence difficulties [24]. Therefore, the SRCNN method reduced training difficulty and the number of training parameters by sharing weights across scales. ConvLSTM, which connected adjacent scales in a hidden state in the middle of each scale, can effectively retain the feature information of the previous scale and improve the performance of the network.

F. Software

MATLAB R2014a was used to build and test L0 model. TensorFlow 1.10 and Python 3.5 were used to build the MSCNN and SRCNN models. The 64-bit Win10 operating system, with Inter Core i5-3470 CPU, 3.2 GHz, 8GB RAM, 500G hard disk as the software platform, was used to perform the analysis.

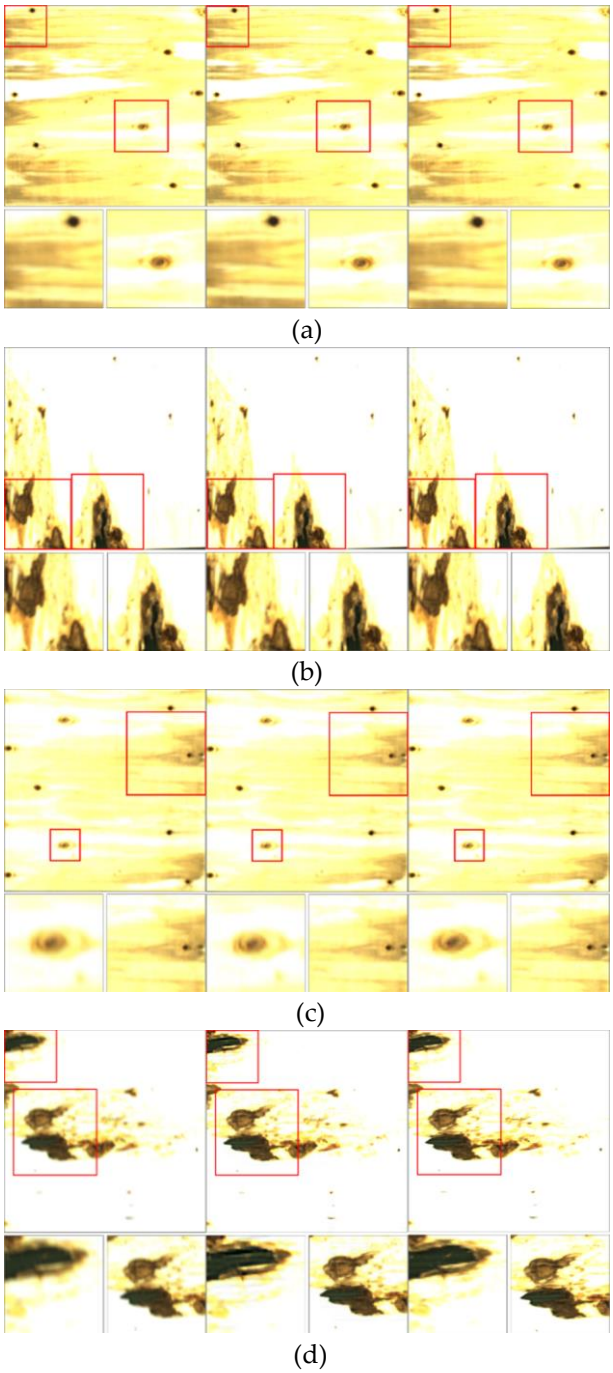

Fig. 7 image restoration test results based on unnatural L0 sparse representation at different speeds (each group of three images represents: blurred image, restored image, and clear image): (a) 50 m/min; (b) 60 m/min; (c) 70 m/min; (d) 80 m/min.

III. Experimental Results and Discussions

In this paper, the effectiveness of the image restoration methods was evaluated by comparing the peak signal-to-noise ratio (PSNR) and the structural similarity (SSIM), which can objectively evaluate image quality more efficiently by virtue of its advantages in calculation amount [25].

A. Wood Veneer Image Restoration Based on Unnatural L0 Sparse Method

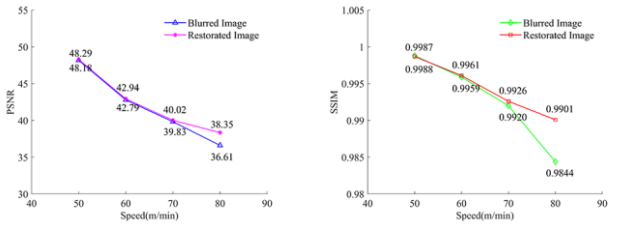

(a) (b)

Fig. 8 image restoration quality comparison based on unnatural L0 sparse representation: (a) peak signal-to-noise ratio; (b) structural similarity.

Based on the multiple sets of reference experiments using static condition (no motion), the optimal blur kernel size (B_S), L0 sparse prior weight (W_L0), regularization parameter (W_R), sparse prior weight (W_S), and other parameters were selected. For conditions with different operation speeds, Table 1 shows the experimental parameter settings of the L0-based image restoration method. Accordingly, L0-based image restoration method was tested on wood veneer image tests with the four different operation speeds. Fig. 7 and Fig. 8 show the analysis results. As shown in Fig. 7, the restoration effect of this L0-based restoration method on the wood veneer image data set was generally poor. A slight restoration effect was shown on the blurred wood veneer image at 80m/min, which reduced the blur of the defect edge, but the blurred veneer image at other speeds was not clearly and intuitively restored. The average increase rate of PSNR compared to the reference condition was less than 0.5% on the fuzzy images for the operation speeds of 50 m/min, 60 m/min, and 70 m/min (Fig. 8). When the operation speed was 80 m/min, the average PSNR growth rate was only 4.74%, while the average SSIM growth rate was less than 1%. In addition, this method had low restoration efficiency for blurry wood veneer images, and it took an average of 1534.5s to restore an image.

Table 1. Parameter Settings of the Image Restoration Method Based on Unnatural L0 Sparse architecture.

Speed	Parameter Value			
	B_S	W_L0	W_R	W_S
50m/min	4	2×10^{-3}	2×10^{3}	0.1
60m/min	4	2×10^{-3}	2×10^{3}	0.1
70m/min	6	2×10^{-3}	2×10^{3}	0.1
80m/min	14	2×10^{-3}	2×10^{3}	0.1

B. Wood Veneer Image Restoration Based on Multi-scale Convolutional Neural Network

The image restoration method based on the MSCNN method did not need to set different parameter values for the blurry wood veneer images under different operation speeds. The MSCNN model obtained through training was tested on the test set containing 624 sets of fuzzy-clear image pairs. Fig. 9 illustrates the image restoration results for this method. At the speed of 70 m/min and 80 m/min, the blurred veneer image effectively reduced the blur of defect edges, but the restoration effect of blurred veneer image at lower speed was not obvious.

When compared with the reference condition, the MSCNN-based image restoration method improved the average PSNR of blurry wood veneer images under different operation

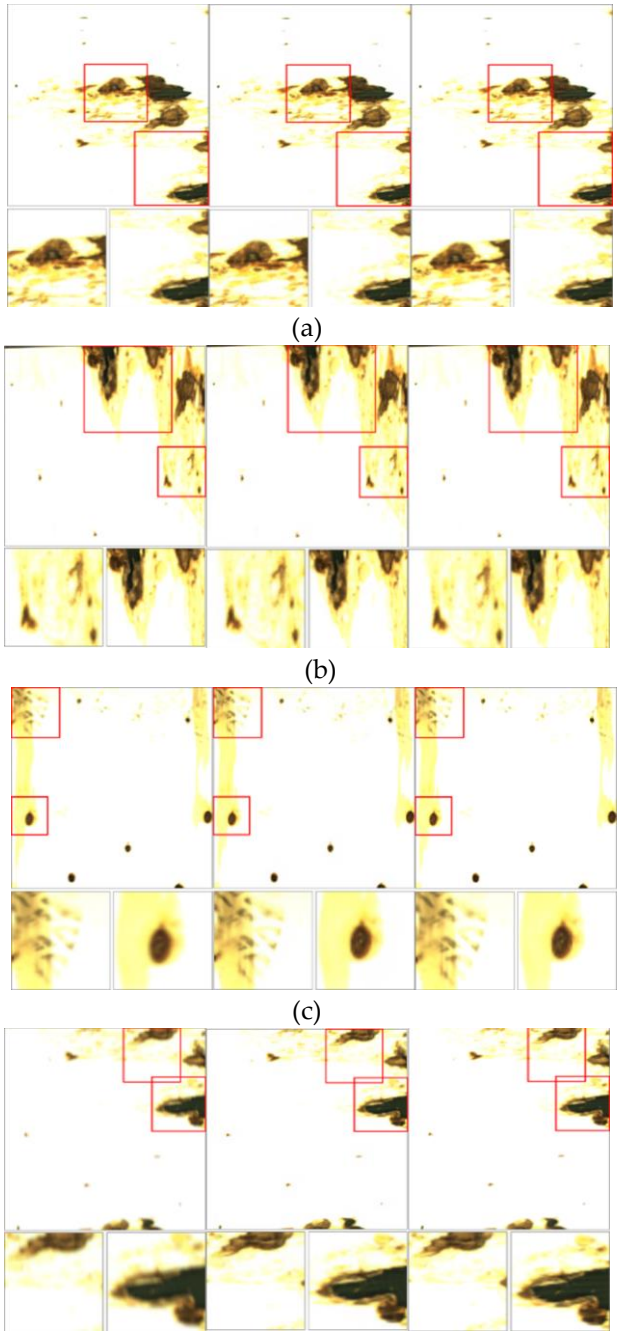

(a) (b) (c) (d)

Fig. 9 image restoration results based on multi-scale convolutional neural network (each group of three images represents: blurred image, restored image, and clear image): (a) 50 m/min; (b) 60 m/min; (c) 70 m/min; (d) 80 m/min.

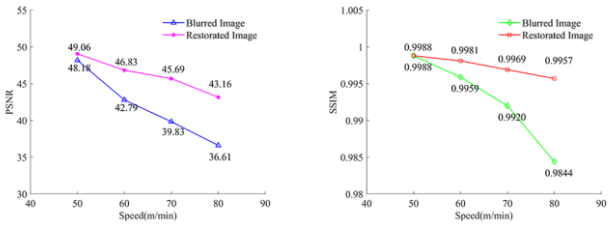

(a) (b)

Fig. 10 image restoration quality comparison based on multi-scale convolutional neural network (a) peak signal-to-noise ratio; (b) structural similarity.

speeds by 1.82%, 9.44%, 14.72%, and 17.88%, respectively. Although it had some restoration effect on the blurry wood veneer image under high-speed operation, the restoration effect on the blurry wood veneer image under low operation speed was insufficient. Moreover, the improvement on the SSIM was also very limited. Only the blurry wood veneer image at 80 m/min had an improvement of 1.15%, while the improvement of the restoration effect at other operation speeds was less than 0.5%. However, the image restoration method based on the MSCNN model significantly improved the efficiency of image restoration, with the average time to restore a blurred veneer image of 21.6 s.

C. Wood Veneer Image Restoration Based on Scale-recurrent Convolutional Neural Network

According to the trained SRCNN model, 624 groups of blur-clear image pairs in the test set were tested for image restoration. Fig. 11 illustrates the results. The blurry image at the operation speed of 50m/min and 60m/min had less blur at the edge of the defect. Although it was restored to a certain extent, the difference in subjective feelings was not obvious. However, the blurring at the edge of defects was more obvious in the blurred images at 70 m/min and 80 m/min. Compared with the blurred image, the texture details of the restored image were closer to a clear image.

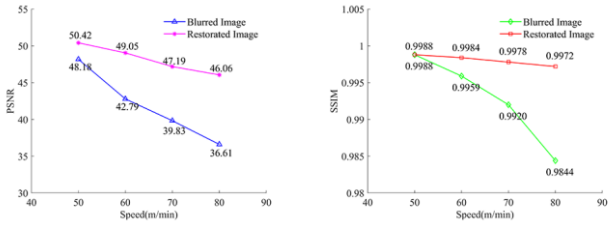

(a) (b)

Fig. 12 image restoration quality comparison based on based on scale-recurrent convolutional neural network: (a) peak signal-to-noise ratio; (b) structural similarity.

Fig. 12 compares the PSNR and SSIM obtained from the SRCNN model with the reference. As the operation speed of the wood veneer increased, the image noise became larger, and the PSNR of the blurred image was reduced. Because the structural characteristics of the image changed less, the SSIM of the blurred image decreased slowly. The SRCNN had a good restoration effect for blurry wood veneer images under different operation speeds. Although the average PSNR increased by

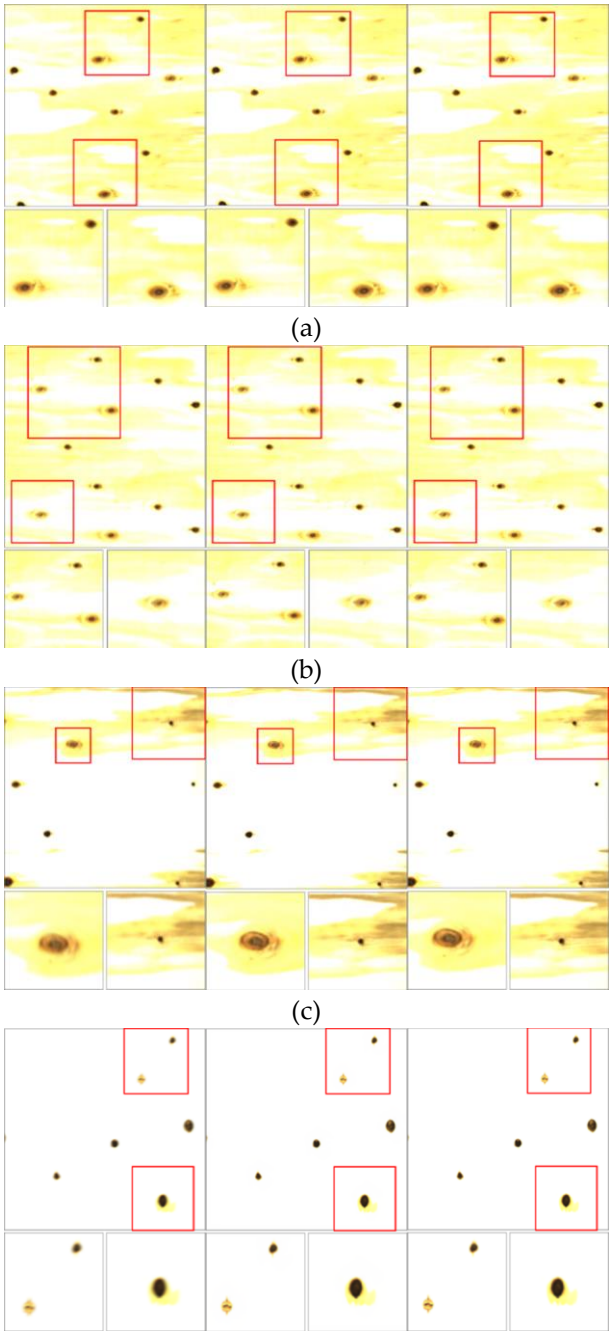

(a) (b) (c) (d)

Fig. 11 image restoration results based on scale-recurrent convolutional neural network (each group of three images represents: blurred image, restored image, and clear image): (a) 50 m/min; (b) 60 m/min; (c) 70 m/min; (d) 80 m/min.

only 4.64% at a moving speed of 50 m/min, it was increased by 14.63%, 18.48%, and 25.79%, respectively, compared to the reference conditions on the blurry wood veneer images at 60 m/min, 70 m/min, and 80 m/min operation speeds. The image restoration ability of SSIM was not obvious, which performed that the improvement of it under different motion speeds was less than 2%. However, Fig. 12 shows that although the structural characteristics of the blurry wood veneer image changed little, the restoration of SRCNN makes the structure of the restored image and the clear image more consistent. The

SRCNN method further improved the operating efficiency to an average of 13.4 seconds to restore a blurry wood veneer image.

D. Discussions

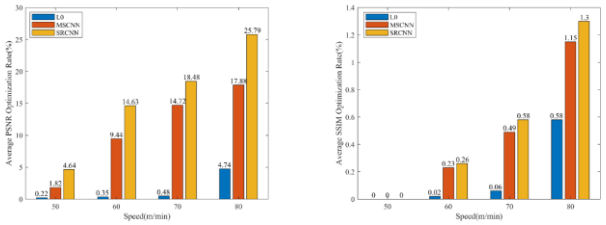

(a) (b)

Fig. 13 comparison of image quality optimization rates of different image restoration methods.

Fig. 13 compares the experimental results of the image restoration method from all the three machine learning methods, including the L0, MSCNN, and SRCNN methods. The traditional image restoration method based on the approximate L0 norm is inefficient with a longer restoring time of 1534.5s, which is much higher than the other two image restoration methods. In terms of the restoration effectiveness of the blurred veneer image, the image restoration method based on the approximate L0 norm is also less than the other two methods. Also the process of the L0 method is more complex, the parameter values need to be adjusted for under different operation speeds, while the other two methods do not need to change these values under different operation speeds.

Between the MSCNN and SRCNN models, by optimizing the network structure, the latter has fewer network parameters and higher operating efficiency with the average time to restore a blurred veneer image reduced by 38%. Due to the addition of the ConvLSTM, the features in the veneer image are more efficiently, and the latter can achieve a better restoration effect for the blurred veneer image under low operation speed motion. Both the MSCNN and SRCNN methods can be applied to the real-time detection system of veneer defects in high operation speed to improve the accuracy of defect type recognition and defect area estimation.

IV. Conclusions and Future Work

This paper compares the effectiveness of three different machine learning methods, including the L0, MSCNN, and SRCNN methods, for the real-time detection system of wood peeling veneer surface defects with different operation speeds. Based on the findings of this paper, following conclusions can be made:

(1) Through comparison between the restoration effectiveness of traditional image L0 restoration method and the neural network-based image restoration methods, it can be seen that since the L0 method needs to solve the fuzzy kernel iteratively, and then restore the image through deconvolution, the error introduced by solving the fuzzy kernel reduces the effectiveness of image restoration. The MSCNN algorithm directly solves the nonlinear mapping between the blurred image and the clear image in an end-to-end method, which effectively improves the quality of image restoration and also has higher computation efficiency. The neural network-based image restoration method showed better restoration results and less time-consuming than traditional image restoration methods.

(2) The MSCNN method uses the structure of stacked residual blocks in each scale. Although the depth of the network was improved, there were too many network parameters too many to estimate, and the texture features between different scales were not sufficient, so only the blur list under low operation speed was restored. The effect of the board image was not good. By optimizing the structure in each scale into a codec network based on residual blocks and adding ConvLSTM in the middle of each scale, the SRCNN method showed improved performance of fuzzy veneer images. The restoration effectiveness and the computing efficiency of the network was significantly enhanced.

Since these conclusions were made based on the limited testing conditions, further researches are needed to expand the single board image data set. As the background information of the veneer image itself is relatively simple, the texture details are not rich enough, which limits the training effect of the neural network. Selecting single-board images with more variety of defects and richer texture details, or collecting moving images of other objects through the single-board image acquisition system to expand the single-board image data set is a direction that can be improved in the next step. In addition, the network structure can be further optimized. As the improved multi-scale convolutional neural network still contains hundreds of convolutional layers, although the parameter sharing method is adopted, the huge network parameters still make it very difficult to train the network. On the premise that the network's receptive field remains unchanged, designing a more optimized structure to reduce network parameters is also needed for further improving the detection effectiveness and efficiency.

Acknowledgment

This study was financially supported by National Key R&D Program of China (Grant No. 2018YFD0600304).

References

[1] Food and Agriculture Organization of the United Nations (FAO) (2017). Yearbook of International Environmental Law 28, 506-520

[2] Liao, T. C., Huang, J. H., and Wang, Z. (2020). “Restoration of motion blurred image based on improved inverse filtering model,” Int. Core J. Eng. 6(9), 378-385. DOI: 10.6919/ICJE.202009_6(9).0048

[3] He, Y. Y., Wang, H. L., Feng, L., and You, S. H. (2020). “Motion-blurred star image restoration based on multi-frame superposition under high dynamic and long exposure conditions,” J. Real-Time Image Proc. DOI: 10.1007/s11554-020-00965-0

[4] Xu, L., Zheng, S. C., Jia, and J. Y. (2013). “Unnatural L0 sparse representation for natural image deblurring,” in: Proceedings of the IEEE Conference on Computer Vision

and Pattern Recognition (CVPR), Portland, OR, USA, pp. 1107-1114.

[5] Li, L., Kan, J. M., and Li, W. B. (2014a). "Image denoising via robust simultaneous sparse coding," J. Comput. 9(6), 1418-1425. DOI: 10.4304/jcp.9.6.1418-1425

[6] Li, L., Zhang, R. T., Kan, J. M., and Li, W. B. (2014b). "Image deblurring via an adaptive dictionary learning strategy," J. Inf. Sci. Eng. 12(4), 855-864. DOI: 10.12928/TELKOMNIKA.v12i4.532

[7] Jain, V., and Seung, H. S. (2008). "Natural image denoising with convolutional networks," in: Proceedings of the Twenty-Second Conference on Neural Information Processing System, Vancouver, British Columbia, Canada, pp. 769-776.

[8] Lan, M. C., and Li, C. F. (2018). "Image restoration based on hybrid neural network," Comput. Eng. Appl. 54(09), 201-206. DOI: 10.3778/j.issn.1002-8331.1611-0405

[9] Li, Y., Xu, Q. K., and Li, K. D. (2020). "New method of residual dense generative adversarial networks for image restoration," J. Chinese Comput. Syst. 41(04), 830-836. DOI: CNKI:SUN:XXWX.0.2020-04-030

[10] Koh Jaihyun,Lee Jangho,Yoon Sungroh. Single-image deblurring with neural networks: A comparative survey[J]. Computer Vision and Image Understanding,2021,203.

[11] Engineering; Research Conducted at Chongqing University Has Updated Our Knowledge about Engineering (Deep Pyramid Generative Adversarial Network With Local and Nonlocal Similarity Features for Natural Motion Image Deblurring)[J]. Journal of Engineering,2020.

[12] Xu, L., Lu, C. W., Xu, Y., and Jia, J. Y. (2011). "Image smoothing via L0 gradient minimization," ACM T. Graphic. 30(6), 1-12. DOI: 10.1145/2070781.2024208

[13] Franti, E., Ispas, I., Dragomir, V., Dascalu, M., Zoltan, E., and Stoica, I. C. (2017). "Voice based emotion recognition with convolutional neural networks for companion robots," Rom. J. Inf. Sci. Tech. 20(3), 222-240.

[14] Javaran, T. A., Hassanpour, H., and Abolghasemi, V. (2019). "Blind motion image deblurring using an effective blur kernel prior," Multimed. Tools Appl. 78(16), 22555-22574. DOI: 10.1007/s11042-019-7402-1

[15] Zhuge, Y., Ning, H., Mathen, P., Cheng, J. Y., Krauze, A. V., Camphausen, K., and Miller, R. W. (2020). "Automated glioma grading on conventional MRI images using deep convolutional neural networks," Med. Phys. 47(7), 3044-3052. DOI: 10.1002/mp.14168

[16] Nsh, S., Kim, T. H., and Lee, K. M. (2017). "Deep multi-scale convolutional neural network for dynamic scene deblurring," in: Proceedings of the IEEE Conference on Computer Vision and Pattern Recognition (CVPR), Honolulu, HI, USA, pp. 3883-3891.

[17] Liu, P. F., Zhao, H. C., and Cao, F. D. (2019). "Blind deblurring of noisy and blurry images of multi-scale convolutional neural network," Infrared Laser Eng. 48(04), 300-308. DOI: 10.3788/IRLA201948.0426001

[18] Jia, R. M., Qiu, Z. Z., Cui, J. L., and Wang, Y. D. (2019). "Deep multi-scale encoder-decoder convolutional network for blind deblurring," J. Comput. Appl. 39(09), 2552-2557. DOI: 10.11772/j.issn.1001-9081.2019020373

[19] Denton, E., Chintala, S., Szlam, A., and Fergus, R. (2015). "Deep generative image models using a Laplacian Pyramid of adversarial networks," in: Proceedings of the 28th International Conference on Neural Information Processing Systems (NIPS), Montreal, Canada, pp.1486-1494.

[20] Eigen, D., and Fergus, R. (2015). "Predicting depth, surface normals and semantic labels with a common multi-scale convolutional architecture," in: 2015 IEEE International Conference on Computer Vision (ICCV), Santiago, Chile, pp. 2650-2658.

[21] Mathieu, M., Couprie, C., and Lecun, Y. (2016). "Deep multi-scale video prediction beyond mean square error," in: 2016 International Conference on Learning Representations (ICLR), San Juan, Puerto Rico.

[22] Rezaei, H., Aertsen, A., Kumar, A., and Valizadeh, A. (2020). "Facilitating the propagation of spiking activity in feedforward networks by including feedback," PLoS Comput. Biol. 16(8). DOI: 10.1371/journal.pcbi.1008033

[23] Tao, X., Gao, H. Y., Shen, X. Y., Wang, J., and Jia, J. Y. (2018). "Scale-recurrent network for deep image deblurring," in: 2018 IEEE/CVF Conference on Computer Vision and Pattern Recognition, Salt Lake City, UT, USA, pp. 8174-8182.

[24] Shi, X. J., Chen, Z. R., Wang, H., Yeung, D. T., Wong, W. K., and WOO, W. C. (2015). "Convolutional LSTM network: A machine learning approach for precipitation nowcasting," Advances in Neural Information Processing Systems 28, 802-810. DOI: 10.1007/978-3-319-21233-3_6

[25] Gu, J., Meng, G. F., Xiang, S. M., and Pan, C. H. (2019). "Blind image quality assessment via learnable attention-based pooling," Pattern Recogn. 91, 332-344. DOI: 10.1016/j.patcog.2019.02.021

Peng Yuan is currently master student of Mechanical Engineering in the School of Technology, Beijing Forestry University. Before that, he received his B.S. degree from Beijing Forestry University. His research interests are artificial intelligence, machine vision, seed viability assessment, and so on.

Liming Lou is currently a master student of Mechanical Engineering in the School of Technology, Beijing Forestry University. Before that, she received her B.S. degree in Automation from Beihang University. Her main research interests focus on deep learning, computer vision, especially for smoke image analysis.

Yu Shi is currently a Ph.D. student at Beihang University. He received his master degree in Mechatronics Engineering and his B.S. degree in Automation from Beijing Forestry University. His research interests include Machine vision, artificial intelligence, image processing, machine learning, and deep learning.

Pengle Cheng received the Ph.D. degree from Beijing Institute of Technology in 2007. He is currently an Associate Professor with the School of Technology, Beijing Forestry University. His

research interests include artificial intelligence, deep learning, pattern recognition.

Lei Yan is currently a Professor with the School of Technology, Beijing Forestry University, Beijing, China. His research interests include machine vision, pattern recognition, seed nondestructive testing, gait recognition, and so on.

Lei Pang received the B.Eng. degree from the North University of China, Taiyuan, China, in 2016. She is currently pursuing the Ph.D. degree with the School of Technology, Beijing Forestry University, Beijing, China. Her research interests include pattern recognition, hyperspectral image processing, machine learning, and deep learning.